ARTICLE IN PRESS

Journal of Rock Mechanics and Geotechnical Engineering xxx (xxxx) xxx

Contents lists available at ScienceDirect

Journal of Rock Mechanics and Geotechnical Engineering

journal homepage: www.jrmge.cn

Full Length Article

Failure of levees induced by toe uplift: Investigation of post-failure behavior using material point method

Veronica Girardi [a,*], Francesca Ceccato [a], Alex Rohe [b], Paolo Simonini [a], Fabio Gabrieli [a]

[a] University of Padua, Department of Civil, Environmental and Architectural Engineering, Via Ognissanti 39, Padua, Italy
[b] GeoHal, Graswinckelstraat 50, Delft, Netherlands

ARTICLE INFO

Article history:
Received 1 March 2022
Received in revised form
13 May 2022
Accepted 17 July 2022
Available online xxx

Keywords:
Slopes safety assessment
Levees
Uplift pressure
Large deformation analysis

ABSTRACT

Levees are essential structures in flood defense systems, and their failures can lead to devastating consequences on the surrounding territories. One of the failure mechanisms mostly controlled by the foundation soil stratigraphy is the instability of the land side slope, triggered by the development of high uplift pressures in the foundation. This complex phenomenon has been investigated experimentally with centrifuge tests or large-scale tests and numerically with the limit equilibrium method (LEM) and the finite element method (FEM). In this work, we applied a multiphase formulation of the material point method (MPM) to analyze the development of toe uplift instability mechanism, from the onset of failure to large displacements. The numerical model is inspired by an experiment carried out in a geotechnical centrifuge test by Allersma and Rohe (2003). The comparison with the experiment allows for understanding critical pore pressure triggering large displacements in the foundation soils. Moreover, we numerically evaluated the impact of different values of foundation soils' hydraulic conductivity on the failure mechanism. The results show that hydraulic conductivity mainly influences the time of failure onset and the extension of shear localization at depth. Finally, the advantages of using large displacement approaches in the safety assessment of earth structures are discussed. Unlike FEM, there are no issues with element distortions generating difficulties with numerical convergence, allowing for full post-failure reproduction. This capability permits precise quantification of earth structure damages and post-failure displacements. The ensuing reinforcement systems' design is no longer over-conservative, with a significant reduction in associated costs.

© 2022 Institute of Rock and Soil Mechanics, Chinese Academy of Sciences. Production and hosting by Elsevier B.V. This is an open access article under the CC BY-NC-ND license (http://creativecommons.org/licenses/by-nc-nd/4.0/).

1. Introduction

Levees are essential structures in flood defense systems, and their failures can have devastating consequences on the surrounding territories. Levees' failures have different types and their instability mechanisms can be subdivided into hydraulic failures where internal or external erosion processes govern the instability evolution, and macro-instabilities where soil strength reductions control failure triggering. Despite this classification can aid in preliminary recognition, it is far from understanding the complexity of stability analysis and support design in serviceability and ultimate limit state conditions, especially when several physical processes concur to the levee stability. As a water-retention earth structure, levees exhibit a geotechnical behavior strongly controlled by hydromechanical interactions evolving over elapsed time. These interactions depend, for example, on the combination of hydraulic loads, the unsaturated soil state, and the hydromechanical responses, in addition to the heterogeneities of the levee and foundation soils.

One of the failure mechanisms most controlled by the foundation soil stratigraphy is the instability of land side slope triggered by the development of high pressures in the foundation, which is often accompanied by the formation of sand boils. This can occur when there is a foundation layer with high hydraulic conductivity relative to the embankment and in communication with the water basin.

* Corresponding author.
E-mail address: veronica.girardi.1@phd.unipd.it (V. Girardi).

Peer review under responsibility of Institute of Rock and Soil Mechanics, Chinese Academy of Sciences.

https://doi.org/10.1016/j.jrmge.2022.07.015

The development of uplift pressure at the toe of the embankment can lead to failure by triggering two different mechanisms: (i) backward erosion piping, i.e. an internal erosion process due to seepage forces, and (ii) global instability caused by a localized decrease of soil shear strength in the foundation. The focus of the present research work is on the second mechanism.

One of the first documented cases of collapse due to pressure uplift was reported in Cooling and Marsland (1953), who showed that the embankment failure at Dartfort Creek (UK) in 1953 was caused by the development of high pore-water pressure in the underlying layers of permeable sandy gravel. In the Netherlands, the failures of Wolpherense dike in 1981 and Streefkerk dike in 1984 could be attributed to uplift pressures (Van et al., 2005). Amabile et al. (2020) showed that the large deformations developed at the levee crest of the Adige River near San Floriano (Italy) in 1981 was triggered by pore pressure build-up at the toe. The pore pressure build-up was driven by two-dimensional (2D) seepage effects due to high contrast in permeabilities on the land side. Furthermore, according to Van et al. (2005), the uplift stability mechanism is dominant for more than 50% of the dikes in the Netherlands and the frequency is increasing due to the natural land subsidence and water level rise.

Experimental and numerical approaches have been applied in understanding the toe-uplift failure mechanism, including geotechnical centrifuge tests (e.g. Hird et al., 1978; Padfield and Schofield, 1983; Allersma and Rohe, 2003) and large scale field test (e.g. Koelewijn et al., 2004; Van et al., 2005). In centrifuge tests, the control of geometry, materials, boundary conditions, and the possibility of monitoring displacements with pictures taken from the model side (cross-section of the embankment) allow a better understanding of types of failure mechanism.

Among the numerical tools used to investigate these full-scale test and centrifuge test results, the approaches available are based on the limit equilibrium method (LEM) (Bishop, 1955; Van et al., 2005), and the finite element method (FEM) (Allersma and Rohe, 2003; Redaelli et al., 2011). The factor of safety (FS) is commonly defined as the ratio between the maximum available shear strength and the mobilized shear stress. Using LEM, the FS is generally calculated based on equilibrium of driving and resistance forces assuming an arbitrary shape of the failure surface and rigid-plastic soil behavior. Bishop's method is one of the most widely used LEMs; however, due to the assumption of a circular failure surface, it cannot accurately represent the uplift mechanism. In contrast, Van's method accounts for a non-circular slip surface (Van et al., 2005) and thanks to its simplicity, this method has progressively gained popularity in the geotechnical community. In FEM, the FS calculation is implemented with the strength reduction method (SRM). The failure surface is a result of the model and does not need to be defined a priori as that in LEM because the model considers the stress–strain behavior of the soil (Griffth and Lane, 1999). Koelewijn et al. (2004) observed that there are two main issues in reproducing the toe-uplift failure mechanism with commercial FEM software (e.g. Plaxis): (i) in cases with a safety factor (defined as the vertical weight divided by the water pressure in the sand layer) lower than 1.04 (Van et al., 2005), numerical difficulties occur; and (ii) additional assumptions and parameters are required such as elastic moduli, initial stress state.

Modeling the slope deformation beyond the onset of failure is not possible with both LEM, Van's method and FEM. However, quantifying the deformations occurring in these structures is important for a reliable risk assessment. This requires simulation of large displacements, which is possible using other methods such as material point method (MPM), smoothed particles hydrodynamics (SPH), arbitrary Lagrangian-Eulerian methods (ALE), among others. The MPM is a continuum, particle-based technique suitable to model history-dependent materials (Sulsky et al., 1994) like soils, and the method is very popular in the geotechnical community (e.g. Fern et al. (2019)). In recent years, several multiphase formulations have been proposed to describe the behavior of saturated and unsaturated soils (Abe et al., 2013; Jassim et al., 2013; Martinelli, 2016; Yerro et al., 2015, 2022; Kularathna et al., 2022), and unsaturated MPM was applied to predict the behavior of water retention earth structures (e.g. Ceccato et al., 2019a, 2021; Girardi et al., 2021). In this paper, the toe-uplift instability process is simulated with MPM, showing that the kinematic behavior of the slope can be predicted from failure onset to large displacements. The MPM model refers to as the centrifuge experiment performed by Allersma and Rohe (2003) and the experimental and simulated results are compared with respect to the critical water levels and the associated failure mechanism.

2. Uplift mechanism

Levees failure induced by toe uplift is a macro-instability mechanism triggered on the land side, but in some instances it is able to spread to the entire levee and finally results in a massive collapse of the earth structure. This mechanism occurs in a specific stratigraphic condition, as shown in Fig. 1. In the levee foundation, a layer with high permeability, usually a coarse material, has hydraulic continuity from riverside to land side. When the water level increases, the pressure in the coarse layer rises accordingly, and high excess pressure can be reached if the layer is confined by a low permeability layer. The confining layer, typically a soft material like clay or peat, is characterized by a very low mechanical strength.

As a result of increased pore pressures at the base of the confining layer, the shear strength at this location is significantly reduced. In these conditions, sliding takes place along the interface between the two materials, while uplift near the toe area occurs (see Fig. 1). When the contribution to the sliding resistance from the toe is missing from the overall strength, the levee slope may start translating toward the land side, with displacements of the order of meters (Bezuijen et al., 2005).

It is noted that when the pore pressure at the interface between the coarse and soft layers counterbalances the weight of the soft layer above it, the uplift occurs and a thin space between the two soils is created (visible in Fig. 1) which is then filled with pressurized water. It is conventional to define as uplift length the thin water zone forming between coarse and soft layer, characterized by constant pore pressure which is equal to the overburden of the soft layer. This length was analytically analyzed by Barends (1988) considering stationary and nonstationary flow below the embankment, with infinite or finite extension of the land side. Barends (1988) concluded that the analytical expression provides only an order of magnitude for the uplift length, since it tends to overestimate 25%–100% of the actual length.

The toe-uplift failure mechanism is more likely to occur in high levees, where the high water levels necessary to generate uplift pressures can be reached without overtopping. Moreover, this mechanism occurs in stratigraphic conditions very similar to those characterizing backward erosion piping, but the two mechanisms should not be confused. Backward erosion piping is a type of internal erosion that occurs in coarse soils, such as fine- and medium-sand, including silt fraction as well. The erosion pipe propagates below the embankment towards the upstream side, and free water flowing in the pipe can cause a local reduction in soil strength and an excessive enlargement of the pipe, often followed by embankment failure (Cola et al., 2021). The sand boiling at the land slide during flood is a clear evidence to distinguish this phenomenon from the one under analysis.

Please cite this article as: Girardi V et al., Failure of levees induced by toe uplift: Investigation of post-failure behavior using material point method, Journal of Rock Mechanics and Geotechnical Engineering, https://doi.org/10.1016/j.jrmge.2022.07.015

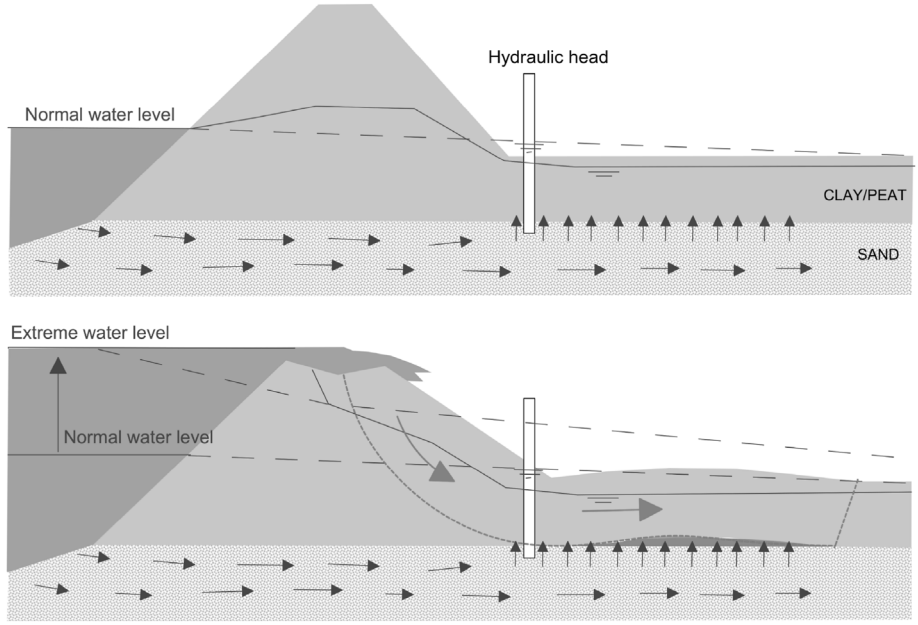

Fig. 1. Schematic process of uplift induced slope failure in the stratigraphic setting of a sand layer under a clay or peat layer in the levee foundation (Adapted from Van et al., 2005).

3. Material point method

The MPM was initially developed for monophase materials in solid mechanics applications (Sulsky et al., 1994), and it was later extended to multiphase mixtures for soil mechanics applications (Abe et al., 2013; Jassim et al., 2013; Martinelli, 2016; Yerro, 2015; Ceccato et al., 2021). In the MPM, two discretizations are presented. On one hand, each continuum body is discretized with a cloud of material points (MPs), which store all material properties, stresses, and kinematic variables. On the other hand, a computational mesh covers the entire domain of potential movement and guarantees the resolution of governing equations at the mesh nodes. A mapping procedure is used to pass information from the mesh nodes and to the MPs and vice versa. Large displacements are simulated as the positions of the MPs are updated independent of the mesh.

At the beginning of a computational step, the material information, kinematic and stress variables are stored in the MPs. Therefore, this information needs to be mapped from the MPs to the background mesh nodes by means of shape functions (Fig. 2a). Then, the momentum balance equations can be solved at the nodes and accelerations (primary unknowns) are obtained (Fig. 2b). The solution of the momentum balance equation system is followed by the update of kinematic quantities at MPs, using interpolation functions. In this manner, it is possible to update strains and stresses (secondary unknowns) at MPs, according to a predefined constitutive model (Fig. 2c). Lastly, the MPs positions are updated, and the mesh is reset to the original location (Fig. 2d).

The behavior of levees and, more generally water retention earth structures, is strongly governed by hydromechanical interactions. When considering the levee body, the unsaturated conditions generally prevail most of the time, while the levee foundation can be either unsaturated or fully saturated in normal conditions. A recent unsaturated formulation proposed by Ceccato et al. (2021) and implemented in the open-source code Anura3D (2022) is used to study the toe-uplift failure mechanism to account for this complex multiphase behavior.

The set of governing equations is the momentum balance of the liquid and of the mixture (Eq. (1) and (2)), the mass balance for liquid and solid (Eq. (3) and (4)), the constitutive law for the liquid which is assumed weakly compressible in Eq. (5), the constitutive model for the solid in incremental form expressed in Eq. (6), and the compatibility equations (Eqs. (7) and (8)):

$$\rho_L \boldsymbol{a}_L = \nabla p_L - \boldsymbol{f}_L^d + \rho_L \boldsymbol{g} \tag{1}$$

$$n_S \rho_S \boldsymbol{a}_S + n_L \rho_L \boldsymbol{a}_L = \mathrm{div}(\boldsymbol{\sigma}) + \rho_m \boldsymbol{g} \tag{2}$$

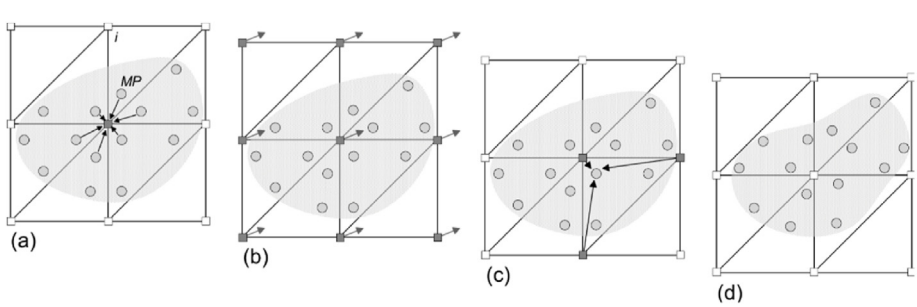

Fig. 2. Computational scheme of MPM: (a) Information mapping to the nodes; (b) Resolution of momentum balance equations at the nodes; (c) MP quantities update; and (d) MP housekeeping update (*i* stands for the node entity).

Please cite this article as: Girardi V et al., Failure of levees induced by toe uplift: Investigation of post-failure behavior using material point method, Journal of Rock Mechanics and Geotechnical Engineering, https://doi.org/10.1016/j.jrmge.2022.07.015

$$\partial(n_S\rho_S)/\partial t + \mathrm{div}(n_S\rho_S\boldsymbol{v}_S) = 0 \tag{3}$$

$$\partial(n_L\rho_L)/\partial t + \mathrm{div}(n_L\rho_L\boldsymbol{v}_L) = 0 \tag{4}$$

$$\partial\rho_L/\partial p_L = -\rho_L/K_L \tag{5}$$

$$\mathrm{D}^s\boldsymbol{\sigma}/\mathrm{D}t = \boldsymbol{D}^{ep}(\mathrm{D}^s\boldsymbol{\varepsilon}/\mathrm{D}t) + \boldsymbol{h}'(\mathrm{D}^s s/\mathrm{D}t) \tag{6}$$

$$\mathrm{D}^s\boldsymbol{\varepsilon}_L\Big/\mathrm{D}t = 1\Big/2\left[\nabla\times\boldsymbol{v}_L + (\nabla\times\boldsymbol{v}_L)^T\right] \tag{7}$$

$$\mathrm{D}^s\boldsymbol{\varepsilon}_S\Big/\mathrm{D}t = 1\Big/2\left[\nabla\times\boldsymbol{v}_S + (\nabla\times\boldsymbol{v}_S)^T\right] \tag{8}$$

where $\boldsymbol{a}_L$ and $\boldsymbol{a}_S$ are the accelerations of the liquid and the solid, respectively; $\boldsymbol{f}_L^d$ is the interaction force between the phases, expressed as $\boldsymbol{f}_L^d = (n_L\mu_L/k_L)(\boldsymbol{v}_L - \boldsymbol{v}_S)$, under the validity of Darcy's law; $n_L = nS_L$ and $n_S = (1-n)$ are the volumetric concentration ratios, in which S_L is the saturation degree and n is the porosity; μ_L is the dynamic viscosity of the liquid and k_L is the intrinsic permeability; $\boldsymbol{v}_L$ and $\boldsymbol{v}_S$ are the velocities of the liquid and the solid, respectively; $\boldsymbol{g}$ is the gravity vector, ρ_L and ρ_S are liquid and solid densities which are used to compute the mixture density; $\rho_m = n_S\rho_S + n_L\rho_L$; K_L is the bulk modulus of the liquid; $\mathrm{D}^s(\cdot)/\mathrm{D}t$ is the material derivative with respect to the solid motion; $\boldsymbol{D}^{ep}$ is the tangent stiffness matrix; $\boldsymbol{h}'$ is a constitutive vector. $\boldsymbol{\varepsilon}$ is the strain tensor; $\nabla = \left(\frac{\partial(\cdot)}{\partial x}, \frac{\partial(\cdot)}{\partial y}, \frac{\partial(\cdot)}{\partial z}\right)^T$ is the operator of partial derivatives, $\times$ indicates the cross product and T indicates the transpose of a vector; p_L is the liquid pressure.

The total stress $\boldsymbol{\sigma}$ is related to the liquid pressure p_L considering Bishop effective stress principle (Eq. (9)):

$$\boldsymbol{\sigma} = \boldsymbol{\sigma}' + S_L p_L \boldsymbol{m} \tag{9}$$

where $\boldsymbol{m}$ is a unit vector, $\boldsymbol{\sigma}'$ is the effective stress and the saturation degree S_L is a function of suction using the soil water retention curve (SWRC).

The hydraulic model consists of the SWRC and the hydraulic conductivity curve (HCC), the latter expresses hydraulic conductivity as a function of the saturated hydraulic conductivity and degree of saturation. Detailed explanations about the SWRC and HCC implemented in Anura3D can be found in previous studies (e.g. Ceccato et al., 2021; Girardi et al., 2021). Eqs. (1) and (2) are discretized in space using the Galerkin approach and solved for the nodal accelerations. Eqs. (3)-(8) are solved at the MP level. The semi-explicit Euler-Cromer time discretization scheme is adopted and the critical time step size is determined according to the studies of Mieremet (2015) and Yerro et al. (2022).

Boundary conditions for the solid are fixities and tractions, while for the liquid are impermeable boundaries, pressures or total heads, rainfall/evaporation, and potential seepage face. The potential seepage face is applied at the borders where it is unknown whether the condition is a flux or a pressure. With this condition, the liquid can flow out of the soil at zero pressure and cannot enter in unsaturated conditions. Additional information on implementation strategies related to each condition can be found in Ceccato et al. (2021).

4. Investigation of levee failure and post-failure with centrifuge tests and MPM simulations

4.1. Baseline physical test

In this section, we introduce the physical test used as a reference to apply MPM in the study of the toe uplift mechanism. The reference experiment is part of a series of tests conducted by Allersma and Rohe (2003) in a geotechnical centrifuge at Delft University of Technology, in 2003. These experiments aim at reproducing in a controlled environment the conditions triggering toe uplift collapse mechanism, in order to improve our understanding of the phenomenon. The presence of berms and trenches is tested experimentally. The standard dike test (without reinforcement systems) is considered here as a reference for the MPM model.

In the centrifuge test, the levee is built at the model scale, with dimensions reported in the sketch of the experimental configuration in Fig. 3 (dimensions of the levee at prototype scale are also added in parentheses). In the selected case, the levee and the shallow foundation layer are built with the same material (kaolin clay), while the deep layer is made of sand. Strength parameters are computed based on consolidated undrained triaxial tests (see Table 1).

The reservoir (in Fig. 3 referred to as water tank) representing the riverside is progressively filled with water; this is hydraulically disconnected from the levee body due to the presence of a plastic membrane that prevents seepage in the levee body and in the clay foundation. The reservoir is connected to the deep sandy layer with a tube. A small vertical polystyrene wall is placed on top of the levee, allowing water levels higher than the levee's crest to generate higher pressure in the sand layer. At the other end of the layer, the total head in the sand is controlled with a height-adjustable drain, at a fixed height of 2 cm above the ground level (Rohe and Allersma, 2000).

The centrifuge is accelerated in steps of 10*g* until the final value of 120*g* is reached in approximately 15 min. The reservoir level is initially half the levee height, and it is progressively raised to the maximum value, along with the gravity increment. From the pictures of the experiment (Fig. 4c), it shows that the maximum level (H) is between 6.5 cm and 7 cm.

The evolution of collapse is displayed in the centrifuge test with respective gravity levels (see Fig. 4). This graphical representation (adapted from Rohe and Allersma (2000)) is done by subtracting greyscale values of the current phase from the previous phase to

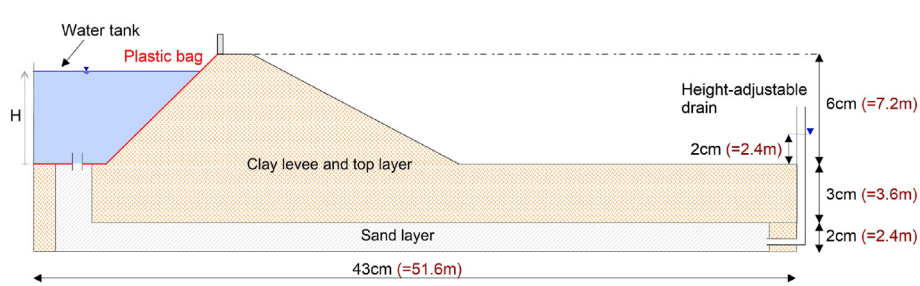

Fig. 3. Sketch of the principal features of the baseline centrifuge test (model scale). The dimensions at prototype scale are reported in parentheses in red.

Please cite this article as: Girardi V et al., Failure of levees induced by toe uplift: Investigation of post-failure behavior using material point method, Journal of Rock Mechanics and Geotechnical Engineering, https://doi.org/10.1016/j.jrmge.2022.07.015

Table 1
Material parameters for the MPM model of toe uplift induced instability.

Parameter	Sand	Clay
ρ_S (kg/m^3)	2610	2542
ρ_L(kg/m^3)	1000	1000
n	0.355	0.3
K_L (kPa)	60,000	60,000
μ_L (kPa s)	10^{-6}	10^{-6}
a_v(1/kPa)	6×10^{-3}	4×10^{-4}
k_{sat}(m/s)	7.44×10^{-3}	7.44×10^{-5}
E (kPa)	55,860	5520
ν	0.33	0.15
φ' (°)	37	22
c' (kPa)	0	10

highlight deformations. In Fig. 4a, the displacements resulting from accelerating from 1g to 90g are shown. At this step, the slip surface is still not visible and the water level is low (half the dike height). In Fig. 4b, the displacements from 90g to 100g caused by the acceleration can be seen. A sliding mass is now visible, bounded by an active sliding surface. In Fig. 4c, the displacements between 100g and 120g are shown. Meanwhile, the water level has also increased at the height of the crest. A secondary shallow slip plane is created over which the levee slides. Afterward, a passive slip plane arises due to the increasing horizontal deformation. This slip plane forms an approximate straight line. On the right side of this line, no deformation can be recognized anymore.

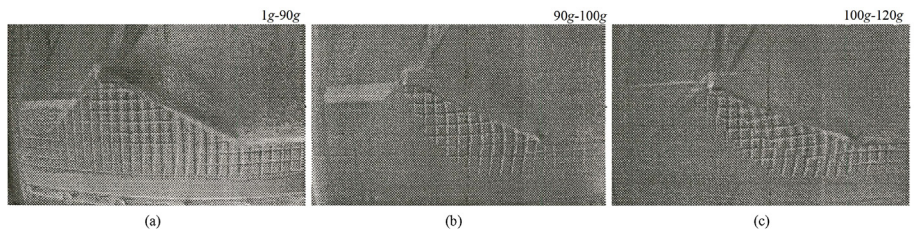

Fig. 4. Relative displacements at three progressive increments of the gravity level in the centrifuge test: (a) 1g–90g; (b) 90g–100g; and (c) 100g–120g (adapted from Rohe and Allersma, 2000).

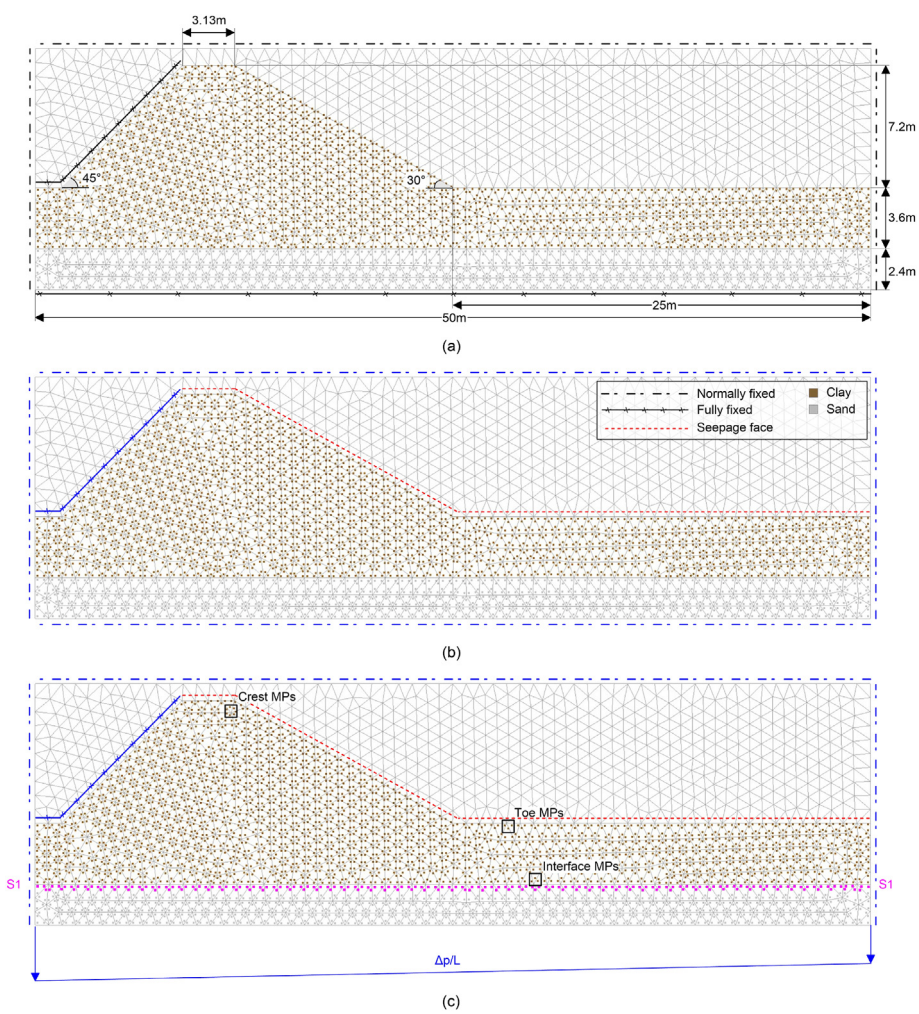

Fig. 5. MPM model of centrifuge test (prototype scale): (a) Boundary conditions for the solid for the entire simulation time; (b) Boundary conditions for the liquid during initialization; and (c) Boundary conditions for the liquid after initialization.

Please cite this article as: Girardi V et al., Failure of levees induced by toe uplift: Investigation of post-failure behavior using material point method, Journal of Rock Mechanics and Geotechnical Engineering, https://doi.org/10.1016/j.jrmge.2022.07.015

Table 2
Boundary values of the imposed nodal pressures at the model bottom.

Phase	Δt (min)	$\overline{p}_L\|_{x=0\ m}$ (kPa)	$\overline{p}_L\|_{x=50\ m}$ (kPa)
1	8	−82	−82
2	45	−102	−82
3	116	−122	−82
4	182	−142	−82
5	202	−162	−82

4.2. Numerical model set up

The MPM model is built considering the main geometrical features of the experiment at the prototype scale, following the well-known similitude ratio in Eq. (10):

$$L_m / L_p = 1/N \tag{10}$$

where N is the amplification factor of gravity, which in the reference experiment assumes a final value of 120; and L_m and L_p are geometrical lengths in the model and the prototype, respectively. Plain strain conditions are assumed. The geometry of the model and the mesh discretization are reported in Fig. 5. The mesh is made of 3-noded triangular elements with an average edge size of 0.8 m. At the beginning of the simulation, 3 MPs are assigned to each element.

The properties of the two materials are listed in Table 1. Liquid bulk modulus K_L is reduced to 60,000 kPa. This assumption is made to speed up the computation and numerical stability. Preliminary analyses showed that the bulk modulus is still sufficiently high to not affect the physics of the phenomenon under analysis. The water retention properties are not reported in the reference paper, so simplified linearized SWRCs (Eq. (11)) are used:

$$S_L = 1 - a_v p_L \tag{11}$$

where a_v is calibration parameter, which is based on the literature for similar materials (Lu and Likos, 2004).

The hydraulic conductivity function for each material is assumed constant (not changing with the saturation degree), equal to the saturated hydraulic conductivity value. In the experiment, the saturated hydraulic conductivity of clay is $k_c = 1.16 \times 10^{-9}$ m/s, while in the numerical model a higher value is used, as reported in Table 1. The final value of clay hydraulic conductivity in Table 1 represents a compromise between minimizing the computational cost and best matching with the experimental outcome. In Section 5, the impact of hydraulic conductivity of the clay layer on the MPM simulation is investigated.

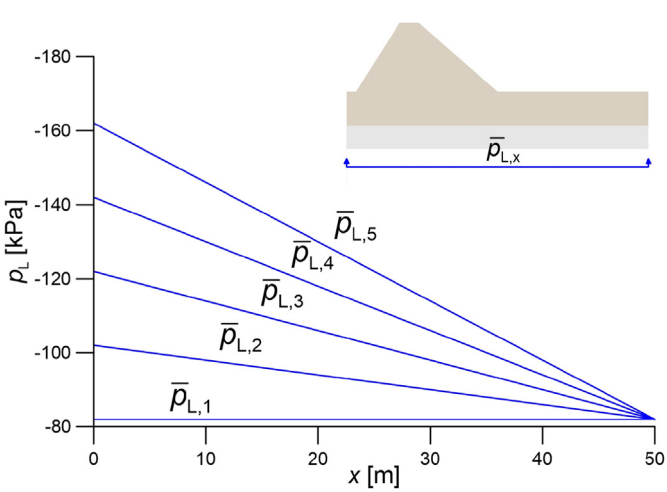

Fig. 6. Imposed nodal pressure along the bottom edge of the model during the five subsequent phases.

An elastic-perfectly plastic Mohr-Coulomb model is used for the soil response of both materials, with parameters based on the experimental values (Allersma and Rohe, 2003). The Young's modulus is selected considering the unloading path which is most representative of the phenomenon under analysis. A mass scaling of 100 is used to reduce the computational cost and a small value of damping, equal to 0.05, is used to guarantee numerical stability (Ceccato et al., 2019b).

The boundary conditions for the solid phase are shown in Fig. 5a, which remain constant for the entire simulation. The choice of fixing the inner slope is related to the experimental configuration, where the reservoir, gradually being filled, acts in a stabilizing manner for the riverside slope, which otherwise would tend to collapse before the maximum water level is reached. The bottom edge of the model is fully fixed, whereas the other lateral edges are normally fixed. Pressure and stress are initialized with the K_0-procedure ($K_0 = 0.5$), assuming that the water table is at the interface between sand and clay. The initial location of the water table guarantees the unsaturated conditions of the levee body and the clay foundation layer. One load step of quasi-static gravity loading is run after the K_0-procedure to improve the stress distribution. During initialization, the bottom is impermeable (see Fig. 5b). The hydraulic boundary condition on the inner slope is impermeable, resembling the plastic membrane effect, while on the land side a potential seepage face is assumed. After initialization, only the bottom boundary condition for the liquid is changed to an imposed pressure (see Fig. 5c). The applied pressure has a linear distribution with a maximum on the left side $\overline{p}_L|_{x=0\ m}$ and a minimum on the right side $\overline{p}_L|_{x=50\ m}$. The first changes in its magnitude during simulation, resembling water table rising in the reservoir, while the latter is constant as the drain height is kept fixed in the experiment. The term "Phase" in the following is used to define a part of the simulation characterized by a specific distribution of nodal pressure at the bottom.

In the MPM model, a uniform initial distribution of imposed nodal pressure equal to −82 kPa is assumed (Phase 1), which corresponds to a water column of 2.4 m above ground level and equals to the height of the drain. This condition is maintained for 8 min. In the MPM code used (Anura3D), compressive stresses have a negative sign, and the same convention stands for pressures (in fact, suctions are positive pressures).

The values at the extreme nodes of the model having the linear distribution, i.e. $x = 0$ m and $x = 50$ m, are reported in Table 2. Each new pressure distribution defines a new phase of the simulation with a certain duration, also reported in Table 2. The horizontal pressure gradient at the bottom boundary tends to become steeper progressively, as displayed in Fig. 6.

From Fig. 4, the position of the maximum water level is identified during the experiment ($H = 7.8–8.4$ m), which corresponds to a pressure of approximately −120 kPa at the interface between sand and clay. This means that the critical pressure distribution capable of triggering the instability should be between Phase 3 and Phase 4. Phase 5 does not have an experimental counterpart and is carried out to numerically explore the evolution of failure in the event of an additional pressure increase.

The MPs near section S1 are highlighted in Fig. 5c. Information is extracted from the S1 MPs to monitor the stresses and pressures at the interface between sand and clay. Furthermore, in the same figure, three locations are selected (crest, interface, and toe) to track the evolution of MPs kinematic variables in the next section.

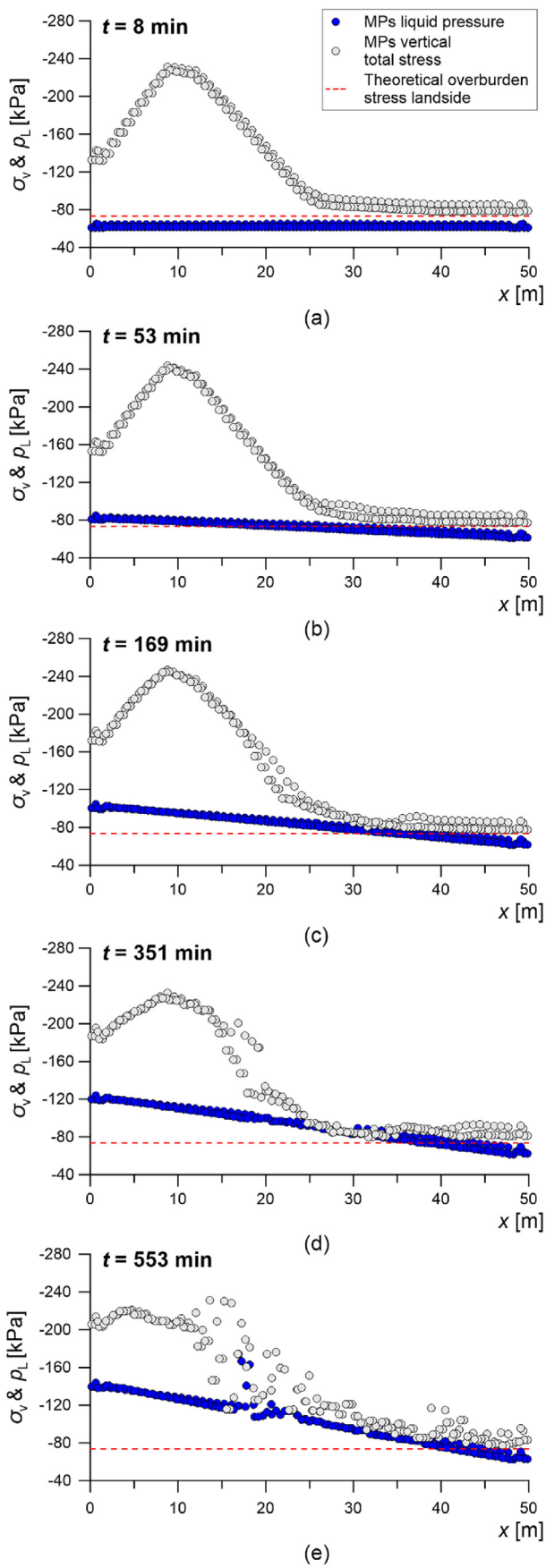

Fig. 7. MPs stress variables along section S1 at five instants, corresponding to the end of each phase: (a) $t = 8$ min; (b) $t = 53$ min; (c) $t = 169$ min; (d) $t = 351$ min; and (e) $t = 553$ min.

4.3. Results

As introduced in the previous sections, the problem under analysis is strongly controlled by three main aspects: stratigraphy, material properties, and variation of hydraulic boundary conditions (mainly the pressure in the sand layer). Among the objectives of the MPM model, we aim at identifying the critical pressure gradient at the interface between sand and clay, triggering failure, and the consequent displacements. These displacements can be completely reproduced by the MPM model, in response to each modification of the boundary conditions.

Figs. 7 and 8 illustrate stress and deformation, respectively. It should be noted that the pressure at the interface between sand and clay does not correspond to the imposed pressure at the bottom. Therefore, it is necessarily decreased by a factor ($\gamma_w h$), where γ_w is the water specific weight and h is the thickness of the sand layer. This pressure, stored at the MPs, is computed along the interface section S1 at each computational step and compared with the total vertical stress along the same section in Fig. 7. The overburden stress on the land side, considering a clay thickness of 3.6 m, outside the load footprint of the levee, is equal to 73.44 kPa. As a reference, this value is reported in Fig. 7 with a horizontal red line.

Each panel of Fig. 7 shows the stresses along S1 corresponding to the end of each phase. It is visible that, starting from $t = 169$ min (end of Phase 3), the liquid pressure values approach the total vertical stress values near the toe between $x = 30$ m and $x = 35$ m, thus uplift occurs. Consequently, a shear failure surface develops, and acceleration of displacements is observed. This is visualized in Fig. 8 which reports contours of deviatoric strain and norm of displacements. At $t = 169$ min, high deviatoric strains are observed near the interface between sand and clay and extend both toward the land side toe and the river side crest.

For the corresponding displacements, the displacement vectors near the land side are oriented upward and toward the land side, with maximum displacements equal to 13 cm. The direction of movement appears as the onset of a rotation. At the same time, along the interface, between $x = 20$ m and $x = 25$ m, vectors are horizontal and directed toward the land side, showing a translational movement. Lastly, the vectors along the surface of the land side show an upward movement. At $t = 170$ min (beginning of Phase 4), pressure increases and the failure process is fully triggered (Fig. 8). At this time, the slip surface is more marked and continuous, with an overall increment of strain. The displacement vectors show that the movement is characterized by a translation in the foundation, near the levee's toe, and a roto-translation of the levee slope. This result is distinctive of the phenomenon under analysis, and well captured by the MPM.

During Phase 4, the process evolves, with displacements even higher than 1 m. Consistently, in the range $25 < x < 35$ m, the total stress and pressure are approximately equal along S1, as visible in Fig. 7 at the end of Phase 4 ($t = 351$ min). The subsequent increment of pressure (Phase 5) triggers additional movements and larger displacements, resulting in a more irregular stress distribution on the land side, with oscillations typical of MPM (see Fig. 7). In Anura3D, stress oscillations are mildly mitigated with the MPM-MIXED procedure, which is also used in the simulations in this study. The MPM-MIXED procedure averages the stresses of all the MPs in an element (Anura3D MPM Research Community, 2022). Although more advanced strategies have been proposed to mitigate stress oscillations (e.g. Steffen et al., 2008; Sadeghirad et al., 2011;

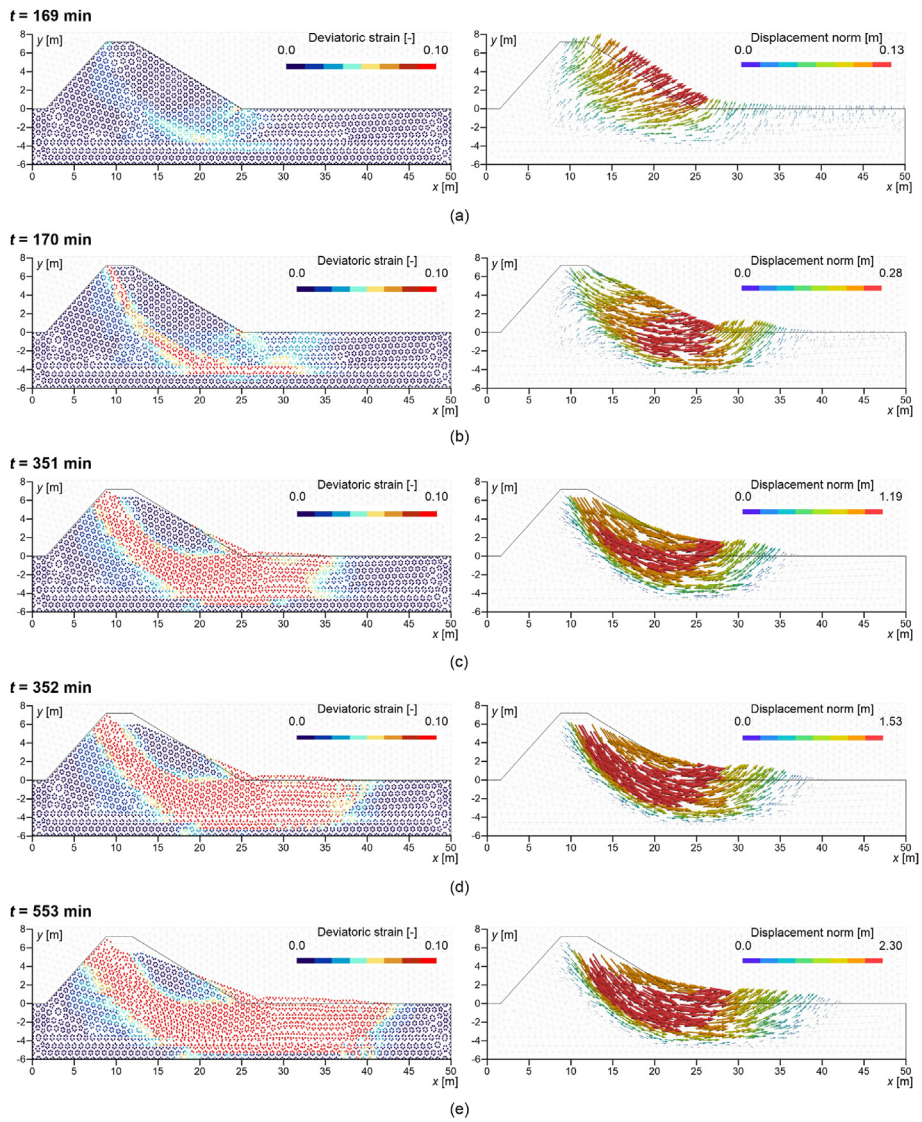

Fig. 8. Contours of deviatoric strain (left column) and norm of displacements (right column) for five instants of time: (a) $t = 169$ min; (b) $t = 170$ min; (c) $t = 351$ min; (d) $t = 352$ min; and (e) $t = 553$ min.

Zhang et al., 2011; González-Acosta et al., 2020), the issue has not been fully solved yet. In the present study it does not seem to impact the key failure mechanism and final displacement.

At the end of Phase 5 ($t = 553$ min), the levee crest of the MPM model settles approximately 2 m, while the toe reaches a vertical displacement of approximately 0.8 m (Fig. 8). These displacements provide a clear picture of the damage to the levee, and this quantification has never been possible until now with other numerical techniques.

The impact of pressure increments of Phases 3, 4, and 5 on the displacements is reported in Fig. 9 with relative displacements. Relative displacements are computed for consecutive instants, thus for instance, relative displacement vectors at $t = 54$ min are obtained by subtracting displacement vectors at $t = 53$ min from displacement vector at $t = 54$ min. With this graphical representation, the increase in the movement due to each new pressure distribution and the progressive development of the instability mechanism is quantifiable. As mentioned above, the pressure distribution of Phase 3 can be defined as "critical"; indeed toe uplift and large translational movements occur at the beginning of this phase.

The dynamic process of levee failure can be additionally analyzed by considering the kinetic energy of the system (Fig. 10a). Two peaks of major intensity can be recognized at approximately $t = 180$ min and 360 min, immediately after applying bottom pressures of Phases 4 and 5. The peaks correspond to a rapid acceleration of the soil masses, in response to the applied pressure. In Fig. 10b, liquid pressure and vertical stresses at MPs on S1 (in the sand layer) with coordinate $x \approx 30$ m are plotted.

Liquid pressure increases in each phase and remains almost constant throughout the phase. For the first three phases, vertical total stress is approximately constant, while effective stress decreases. At $t = 170$ min, the liquid pressure and total stress are approximately equal at $x \approx 30$ m, and the resulting effective stress is nearly zero. As time elapses, the slope deforms, and the total and effective stresses increase in absolute value. A similar process is observed in Phase 5. Mild oscillations are visible in the plots of total and effective stress in corresponding to the increased pressure at the beginning of Phases 4 and 5.

Please cite this article as: Girardi V et al., Failure of levees induced by toe uplift: Investigation of post-failure behavior using material point method, Journal of Rock Mechanics and Geotechnical Engineering, https://doi.org/10.1016/j.jrmge.2022.07.015

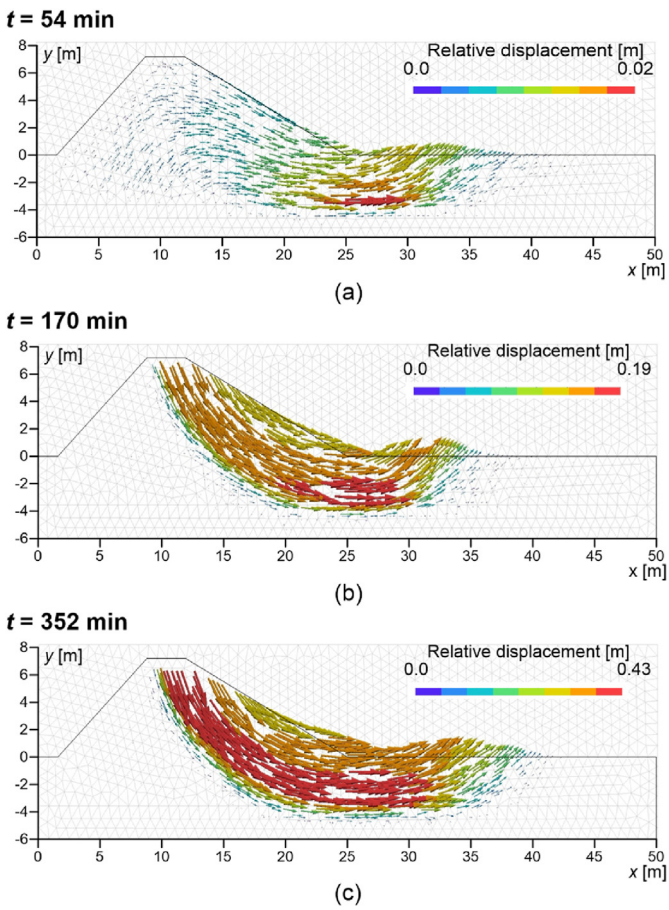

Fig. 9. Relative displacements at three selected instants of time: (a) Passage between Phases 2 and 3 ($t = 54$ min); (b) Between Phases 3 and 4 ($t = 170$ min); and (c) Between Phases 4 and 5 ($t = 352$ min).

In Fig. 10c, the uplift length at prototype scale is computed from the simulation result. The numerical uplift length is computed considering a set of MPs near the interface S1, in a range 11 m $< x <$ 50 m, and evaluating the position of those MPs having vertical effective stress $\sigma_v' \approx 0$. Since $t = 54$ min (Phase 3), the uplift length increases progressively, reaching a maximum value of 7.6 m at $t = 180$ min. This value is very close to the experimental uplift length measured $\sim$ 6 cm (Rohe and Allersma, 2000), corresponding to 7.2 m at the prototype scale (see Fig. 10c). After this peak, during the dynamic motion of the slope, the uplift length oscillates, and it initially decreases during Phase 4, and then increases progressively. During Phase 5, the uplift length reaches a maximum value of 13.5 m, followed by a decrease around the value of 9 m. This response is the result of both numerical and physical factors. In fact, stress oscillations are observed in MPM during the highly dynamic motion and since stresses are used to compute the uplift length, the calculated uplift length oscillates too. Therefore, the computation is indicative and provides a general order of magnitude for Phases 4 and 5, while it is more meaningful in the previous part of the simulation. Concerning the physical aspects impacting on the trend of the uplift length during post-failure, i.e. Phases 4 and 5, it is possible to find an explanation considering Figs. 7 and 10b: during collapse, the effective stress increases again, thus decreasing the uplift length.

Fig. 10d reports the time evolution of some components of displacement δ at three locations (indicated in Fig. 3c): the levee crest, the bottom of the clay, and the toe near the soil surface. These trends help to accurately quantify the large displacements occurring during levee collapse. During Phases 1, 2 and 3, there is a small upward movement due to unloading. But in Phase 4 (i.e. the post-failure stage), the point at the bottom of the clay has a horizontal movement of approximately 0.2 m, and the toe moves upward about 0.5 m, while the crest is settled by 0.6 m. This is important in flood risk management, as it allows quantifying the volume of water poured into the floodplain.

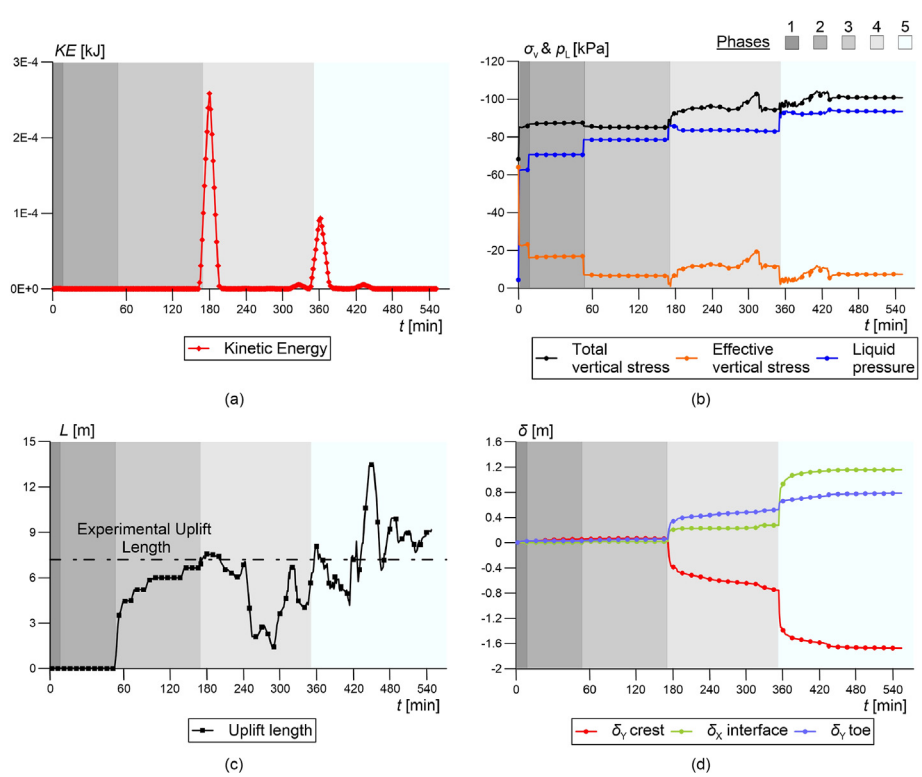

Fig. 10. (a) Time evolution of kinetic energy of the system; (b) Liquid pressure and stress for a MP at the interface between sand and clay (in sand); (c) Time evolution of uplift length; (d) Components of MPs displacement at three locations (negative values stand for settlement of the levee crest).

Please cite this article as: Girardi V et al., Failure of levees induced by toe uplift: Investigation of post-failure behavior using material point method, Journal of Rock Mechanics and Geotechnical Engineering, https://doi.org/10.1016/j.jrmge.2022.07.015

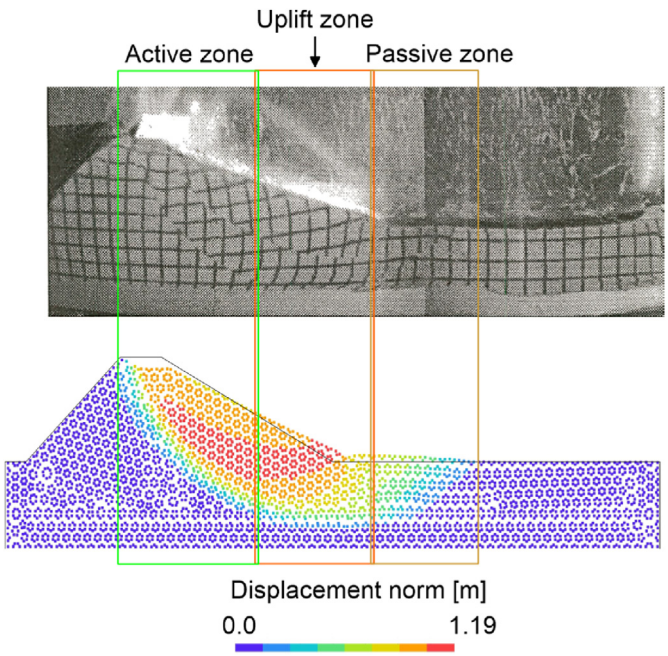

Fig. 11. Comparison between final experimental and numerical configurations.

In Fig. 11, the experimental result is compared with the simulated norm of displacement at the end of Phase 4. As mentioned above, boundary pressures in Phase 5 higher than the experiment are applied to the model, but it is not considered herein. It is possible to identify the typical triple sliding surface composed by the active zone, uplift zone, and passive zone. The extension of the zones is very similar between experiment and numerical results. The magnitude and direction of displacements aid in visualizing the types of movement, showing a rotation in the active area, horizontal translation along the uplift length, and a roto-translation in the passive area.

The shallower slip surface is responsible for some material accumulation at the toe, visible as a small bulging at the end of the slope. This slip surface and its impact on the final profile cannot be accounted for in the MPM model. This is probably due to the difference in the loading path between numerical and experimental models.

In fact, in the experiment, a rise in the amplification factor of gravity with the progressive rise of water level is carried out, while the numerical model is already at the final g-level and only the pressure is progressively increasing. Unlike the numerical model, the initial vertical settlement of the experimental levee after construction may also have impacted on the formation of this shallow slip surface.

5. Effect of permeability ratio on MPM

In the previous section, a higher hydraulic conductivity for the clay layer is assumed to optimize the computational cost. In order to evaluate the impact of this choice, the effect of foundation soils' hydraulic conductivity on the collapse mechanism is investigated in this section. Three different hydraulic conductivity ratios are considered: k_c/k_s equals to 10^{-1}, 10^{-2} and 10^{-3}, where k_c and k_s are saturated hydraulic conductivities of clay and sand, respectively. In each model, k_c is varying, while k_s is kept constant. The ratio between saturated hydraulic conductivity is considered representatively because failure starts at the interface between sand and clay, where the materials are saturated.

Fig. 12 reports the deviatoric strain and liquid pressure contours for three MPM models with different hydraulic conductivity ratios. Deviatoric strain and liquid pressure contours at the beginning of Phase 4 ($t = 170$ min) are presented in Fig. 12. In the investigated cases, high shear strains are initially localized at the interface between sand and clay, and the location of this area is similar. However, the reduction of hydraulic conductivity ratio modifies the

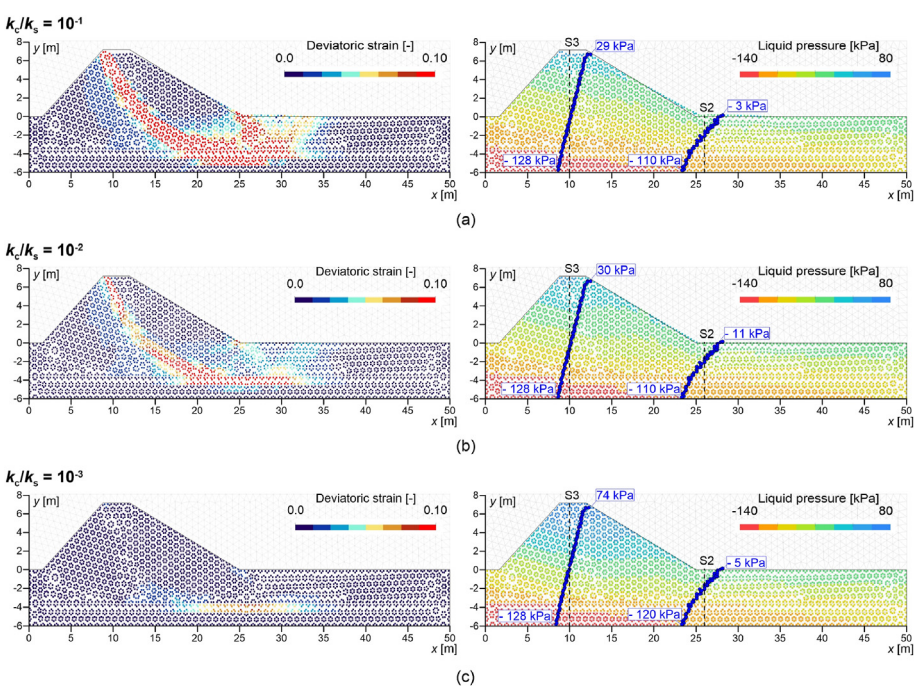

Fig. 12. Impact of hydraulic conductivity on uplift failure mechanism. Deviatoric strain and liquid pressure contours at the beginning of Phase 4 ($t = 170$ min) for numerical models with three different permeability ratios: (a) $k_c/k_s = 10^{-1}$; (b) $k_c/k_s = 10^{-2}$; and (c) $k_c/k_s = 10^{-3}$.

Please cite this article as: Girardi V et al., Failure of levees induced by toe uplift: Investigation of post-failure behavior using material point method, Journal of Rock Mechanics and Geotechnical Engineering, https://doi.org/10.1016/j.jrmge.2022.07.015

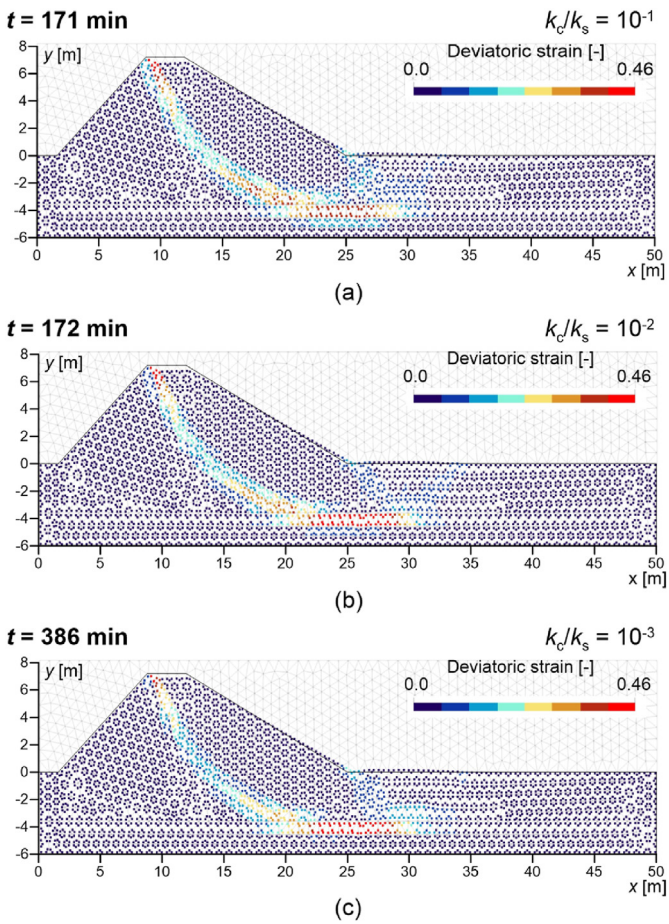

Fig. 13. Onset of failure in terms of deviatoric strain, at different time instants for the three investigated cases of saturated hydraulic conductivity ratio: (a) $t = 171$ min; (b) $t = 172$ min; and (c) $t = 386$ min.

temporal development of the entire slip surface in the active and passive zones. At $t = 170$ min, for $k_c/k_s = 10^{-1}$, the slip surface is well developed on both sides of the levee (Fig. 12). The slope collapse has been triggered, and the crest has settled slightly. In this scenario, the collapse is more rapid and less extended toward the land side. For $k_c/k_s = 10^{-2}$, the slip surface in the passive zone has not yet been clearly developed. For $k_c/k_s = 10^{-3}$, high shear strains are visible only in the uplift zone at this stage, and additional time is necessary to appreciate the entire slip surface formation. The reduction of hydraulic conductivity ratio implies a slower development of the slip surface and evolution of post-failure displacements, plus a slightly more extended uplift length zone.

This behavior is directly linked to the liquid pressure distribution, which depends on the hydraulic conductivity and degree of saturation. To visualize this, the pressure distribution at two sections, S2 and S3, is indicated in Fig. 12. As expected, the sand layer is characterized by similar values in three investigated cases, favoring the localization of shear at depth. On the other hand, the levee body and the clay layer record different values of pressure in the three investigated cases. The higher suctions in the case with smaller hydraulic conductivity ratio ($k_c/k_s = 10^{-3}$) are counteracting the development of the slip surface in the levee body. This phenomenon is of transient nature and the hydraulic conductivity of the clay layer seems to be playing a major role in delaying the progression of movement.

Hydraulic conductivity strongly impacts the time of failure onset and also the speed of progression of the subsequent post-failure. In fact, in Fig. 13, all three investigated cases appear to show a similar slip surface at different times. This is probably due to the fact that uplift begins at the interface between sand and clay due to pressure build-up, then a circular failure surface develops on the levee, where the shear strength is influenced by partial saturation. In the considered experiment, the levee is protected with a plastic membrane, preventing seepage to occur in the levee body and in the shallow foundation soil, thus suction does not change significantly. In real situations, the progressive saturation of the levee body, being potentially also affected by rainfall and the history of water level, may influence the failure mechanism. This aspect requires further detailed investigation, which is out of the scope of this study.

6. Van's method and FEM analysis

In this section, the uplift problem is investigated with the most commonly used approaches in the state-of-practice, i.e. Van's method and FEM, and the advantages and disadvantages of these approaches are discussed.

6.1. Van's method analysis

The stability of river levees with respect to toe uplift can be investigated applying the Van's method, based on the limit equilibrium approach (Van et al., 2005). A scheme is reported in Fig. 14, clarifying the meaning of symbols. The FS is computed by solving the horizontal force equilibrium in Eq. (12):

$$I_a + I_p + F_s = 0 \tag{12}$$

where I_a and I_p are the interslice forces of the active and passive zones, respectively; and F_s is the friction resistance along the straight segment. I_a and I_p are supposed to act at 1/3 height of the beam segment above the sliding plane and are computed considering the moment equilibrium according to Bishop's method.

For $R1 = R2$ and $L = 0$, a completely circular slip plane is obtained, and Van's Method reduces to Bishop's method. The software D-Stability (2021) is used here to calculate the FS for the different loading phases considered in the MPM simulation. The slope geometry is identical to Fig. 5a, and the uplift pressure is applied assigning a total head level to the sand layer with values corresponding to the applied pressure. A horizontal phreatic surface is applied at the ground level for the clay. Only material unit weight and strength parameters are necessary for this analysis. In particular, above the phreatic surface, it is possible to assign a single value of unsaturated weight, assuming that all the soil masses above the phreatic surface have the same weight during the analysis.

Fig. 15 shows the results obtained with Van's method. In Phase 2, the FS value is greater than 1, thus the slope is stable. In Phase 3, FS is slightly lower than 1, which means that failure could occur. This result agrees with the MPM simulation, in which an increase of kinetic energy and large displacements are observed at the end of this phase. Even lower FSs are obtained for Phases 4 and 5 due to the increase of pressure in the sand layer; these results are not representative of real conditions because the geometry of the slope will change during the collapse, as can be observed with MPM.

The Van's method has the advantage of requiring a limited number of parameters and allows determining the slip surface with the lowest FS (critical slip surface). Since it enforces only force equilibrium disregarding the slope deformation, FS lower than 1 can be obtained as an output, but post-failure displacement cannot be inferred. The consequences of $FS < 1$ in terms of damage to the performances of the earth structure cannot be quantified. In a common practice, $FS < 1$ leads to classifying the levee as unsafe; but

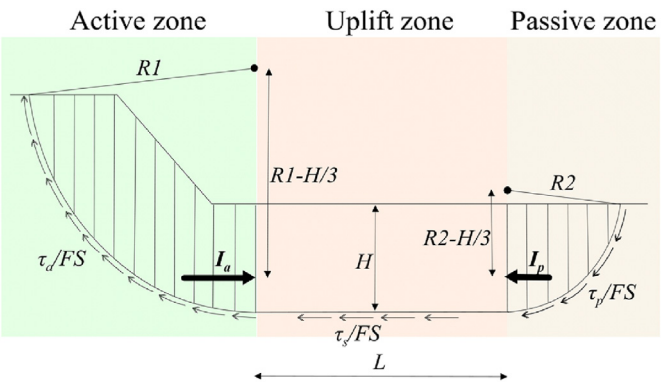

Fig. 14. Triple sliding zone scheme according to Van's Method (adapted from Van et al. (2005)).

in a real scenario, the displacements may be limited, without affecting its normal functioning as shown in Fig. 10. The direct consequence may be an over-conservative design, with associated cost increases. On a positive note, the method is very simple and computationally inexpensive, thus well suited for projects that require a large number of simulations.

6.2. FEM analysis

FEM is a more advanced procedure compared to LEM and it can be used to simulate the progressive increase of pressure in the sand layer below the embankment and the induced deformations up to the onset of failure. Beyond this point, standard Lagrangian FEM will not converge due to excessive element deformation.

In this section, the problem is investigated with the FEM program MIDAS GTS (2020) applying a one-way coupled approach, in which the seepage analysis determines the pressure distribution used in the following non-linear stress analysis to update the stress state and the soil displacements. With this approach, changes in water pressures influence the soil effective stresses, but not vice versa, i.e. soil loading does not generate excess pore pressures. The SRM is applied to determine the FS of the slope.

The slope geometry is identical to the MPM model. The presence of the water reservoir on the left-hand side is simulated with a linear elastic material. The mesh is composed by 6-node triangular and 8-node quadrilateral elements. Discretization and boundary conditions are represented in Fig. 16.

The material parameters are consistent with the MPM simulations, only the permeability of the clay is reduced to 1.18×10^{-9} m/s and it is therefore identical to that in the experiment. In MIDAS GTS NX, a linear distribution of pressure cannot be applied at the bottom of the model as in MPM, thus it is generated with seepage analysis in which appropriate total head levels are applied at the left and right boundaries of the sand layer in order to obtain the same pressure distribution shown in Fig. 6. For Phases 1 and 2, the safety factors obtained with the SRM in these phases are 1.38, and 1.18, respectively. Fig. 17a and b shows the equivalent strain obtained at the end of the stability analysis, and this identifies the failure surface. It can be seen that the failure surface is circular in Phase 1 (Fig. 17a), while in Phase 2, the horizontal sliding surface at the interface between sand and clay is more evident due to the larger uplift pressure (Fig. 17b).

Convergence cannot be reached for Phase 3, when the uplift zone starts to develop, and some elements have zero effective stresses. Therefore, the total head on the left side of the sand layer is progressively reduced to find the closest FEM solution to Phase 3. The maximum pressure at the bottom left corner that brings the model to convergence is 112 kPa, lower than the value applied in MPM simulation (122 kPa). The displacements calculated at the end of this phase are shown in Fig. 17c. The SRM gives a FS of 1.09. The equivalent strain contour plotted in Fig. 17c shows the circular slip surface across the embankment and the horizontal slip surface of the uplift zone, while the circular passive zone is not clearly visible.

The advantage of FEM is that the failure mechanism is the analysis results without assumption like in LEM. The simulation complexity and the computational cost are higher than LEM, but lower than MPM. Unfortunately, stress conditions close to failure and the post-failure behavior of the slope cannot be simulated.

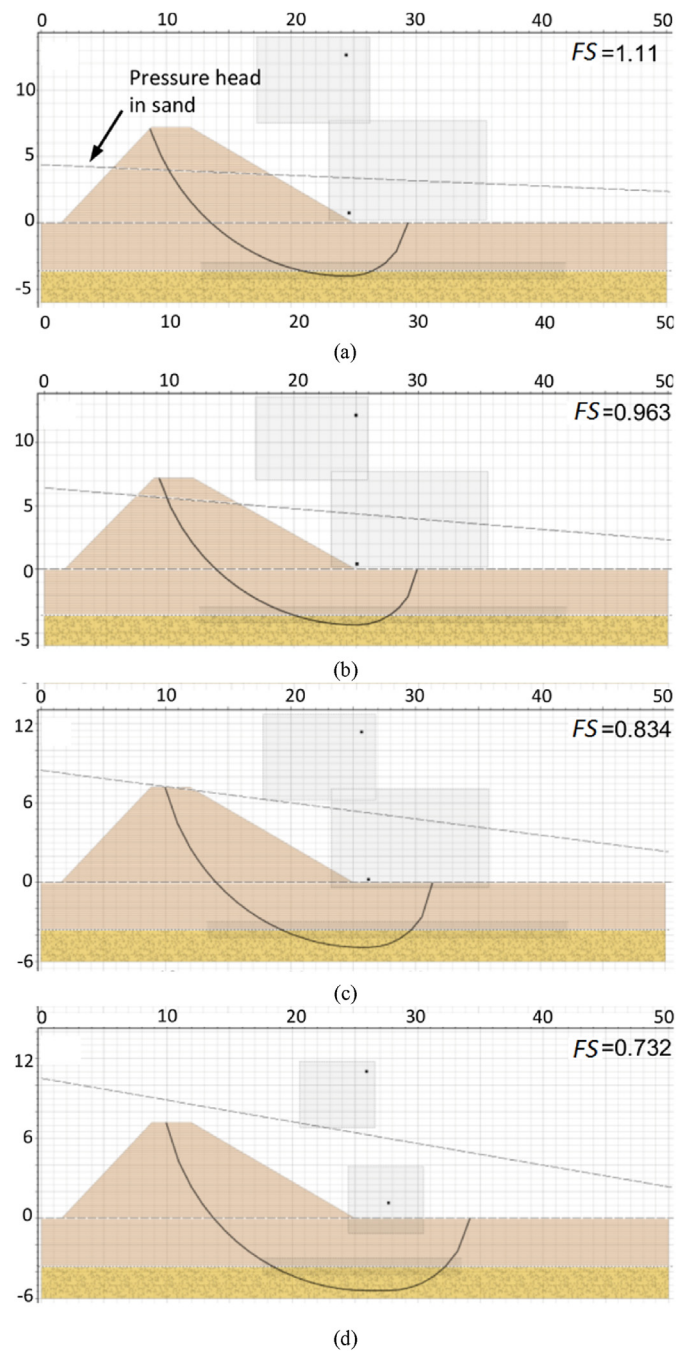

Fig. 15. Slip surface and *FS* with Van's Method for (a) Phase 2; (b) Phase 3; (c) Phase 4; and (d) Phase 5.

Please cite this article as: Girardi V et al., Failure of levees induced by toe uplift: Investigation of post-failure behavior using material point method, Journal of Rock Mechanics and Geotechnical Engineering, https://doi.org/10.1016/j.jrmge.2022.07.015

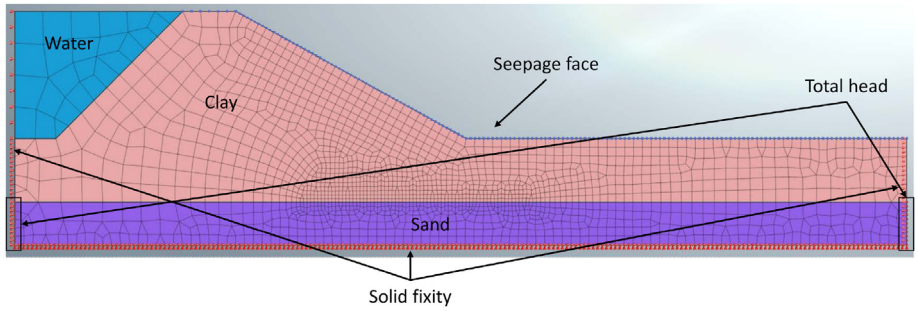

Fig. 16. Discretization and boundary conditions of FEM model.

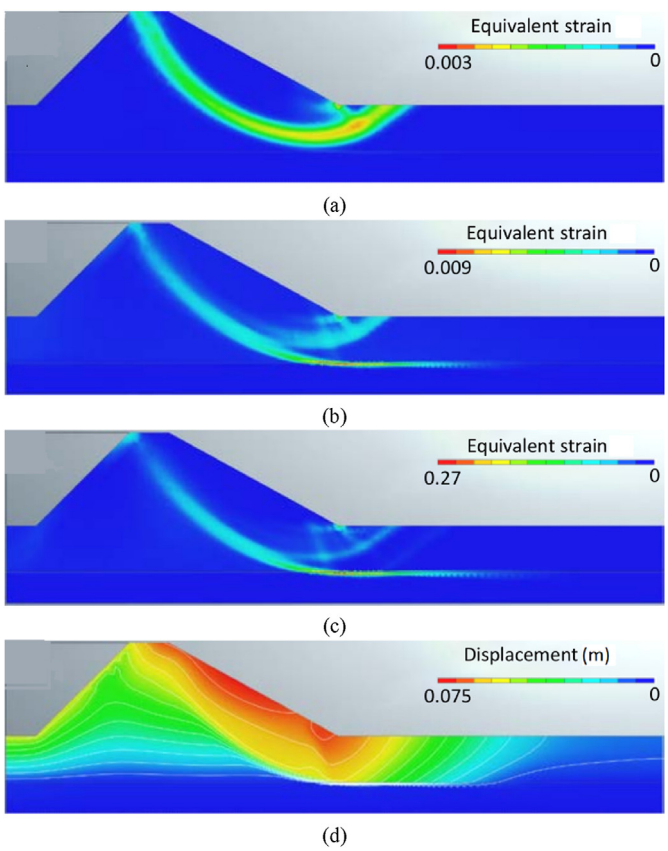

Fig. 17. FEM simulation outcomes: (a) Phase 1: equivalent strain after SRM; (b) Phase 2: equivalent strain after SRM; (c) Phase 3: equivalent strain after SRM; and (d) Phase 3: displacement.

7. Concluding remarks

This work explores the use of a multiphase MPM formulation to assess the safety of levees at risk of uplift failure. Modeling the hydromechanical coupling is fundamental to describe this process.

The method is proved to be an efficient numerical technique for simulating this failure mechanism from the onset of motion to large displacements. The advantages compared to other conventional methods, like Van's method and FEM, are discussed comparing the results obtained simulating the same experiment. The Van's method and FEM can be used up to the onset of failure and tend to be over-conservative in the levee safety assessment, providing $FS < 1$ that may not be directly correlated with large displacements and irreparable damage to the structure of the earth. Moreover, FEM suffers from convergence issues when high gradient of deformations develops, making the final prediction even less reliable. The use of FEM is suggested in combination with MPM: the computational efficiency of FEM allows for the pre-failure investigation, then MPM may be used to describe the entire failure and post-failure.

This study may lay the foundations for the use of MPM for advanced safety assessments of earth structures, providing quantification of slope displacements, thus giving the opportunity to implement optimized protection strategies.

Declaration of competing interest

The authors declare that they have no known competing financial interests or personal relationships that could have appeared to influence the work reported in this paper.

Acknowledgments

Financial supports from University of Padua (Grant No. BIRD181859) and Italian Ministry of Education, University and Research (MIUR), Redreef-PRIN 2017 Call (Grant No. 2017YPMBWJ) are gratefully acknowledged.

References

Abe, K., Soga, K., Bandara, S., 2013. Material point method for coupled hydromechanical problems. J. Geotech. Geoenviron. Eng. 140 (3), 1–16.
Allersma, H.G.B., Rohe, A., 2003. Centrifuge tests on the failure of dikes caused by uplift pressure. Int. J. Phys. Model. Geotech. 3 (1), 45–53.
Amabile, A., Pozzato, A., Tarantino, A., 2020. Instability of flood embankments due to pore-water pressure build-up at the toe: lesson learned from the Adige river case study. Can. Geotech. J. 57 (12), 1844–1853.
Anura3D, 2022. Anura3D MPM Research Community, ANURA3D version 2022 source code. URL: https://github.com/Anura3D/Anura3D_OpenSource. (Accessed 28 July 2022), 2022.
Anura3D MPM Research Community, 2022. Anura3D Scientific Manual version 2022.
Barends, F.B.J., 1988. Uplift of the Hinterland at High Water Levels. Report No. CO-290831/2. GeoDelft, Delft, The Netherlands.
Bezuijen, A., Kruse, G., Van, M.A., 2005. Failure of peat dikes in The Netherlands. In: Proceedings of the 16th International Conference on Soil Mechanics and Geotechnical Engineering (Osaka, Japan).
Bishop, A.W., 1955. The use of the slip circle in the stability analysis of slopes. Geotechnique 5 (1), 7–17.
Ceccato, F., Girardi, V., Simonini, P., 2019a. Developing and testing multiphase MPM approaches for the stability of dams and river embankments. In: Carcaterra, A., Paolone, A., Graziani, G. (Eds.), Proceedings of XXIV AIMETA Conference 2019. AIMETA 2019. Lecture Notes in Mechanical Engineering, pp. 2179–2195.
Ceccato, F., Girardi, V., Yerro, A., Simonini, P., 2019b. Evaluation of dynamic explicit MPM formulations for unsaturated soils. In: Onate, E., Bischoff, M., Owen, D., Wriggers, P., Zohdi, T. (Eds.), Particles 2019 (Barcellona, Spain).
Ceccato, F., Yerro, A., Girardi, V., Simonini, P., 2021. Two-phase dynamic MPM formulation for unsaturated soil. Comput. Geotech. 129, 103876.
Cola, S., Girardi, V., Bersan, S., Simonini, P., Schenato, L., De Polo, F., 2021. An optical fiber-based monitoring system to study the seepage flow below the landside toe of a river levee. J. Civ. Struct. Health Monit. 11, 691–705.

Cooling, L.F., Marsland, A., 1953. Soil mechanics studies of failures in the sea defence banks of Essex and Kent. In: Conference on the North Sea Floods of January 31-February 1, pp. 58–73.
D-Stability, 2021. D-Stability-computer software, v. 2021-02. URL: https://www.deltares.nl/en/software/d-stability/. (Accessed 28 July 2022).
Fern, J.E., Rohe, A., Soga, K., Alonso, E.E., 2019. The Material Point Method for Geotechnical Engineering: A Practical Guide. CRC Press.
Girardi, V., Yerro, A., Ceccato, F., Simonini, P., 2021. Modeling deformations in water retention structures with unsaturated material point method. Proc. Inst. Civil Eng. Geotech. Eng. 174 (5), 577–592.
González-Acosta, J.L., Vardon, P.J., Remmerswaal, G., Hicks, M.A., 2020. An investigation of stress inaccuracies and proposed solution in the material point method. Comput. Mech. 65, 555–581.
Griffth, D.V., Lane, P.A., 1999. Slope stability analysis by finite elements. Geotechnique 49 (3), 387–403.
Hird, C.C., Marsland, A., Schofield, A.N., 1978. The development of centrifugal models to study the influence of uplift pressures on the stability of a flood bank. Geotechnique 28 (1), 85–106.
Jassim, I., Stolle, D., Vermeer, P.A., 2013. Two-phase dynamic analysis by material point method. Int. J. Numer. Anal. Methods GeoMech. 37, 2502–2522.
Koelewijn, A.R., Hoffmans, G., Van, M.A., 2004. Lessons learned from a full-scale dyke failure test. In: Fifth International Conference on Case Histories in Geotechnical Engineering (New York).
Kularathna, S., Liang, W.J., Zhao, T.C., Chandra, B., Zhao, J.D., Soga, K., 2022. A semi-implicit material point method based on fractional-step method for saturated soil. Int. J. Numer. Anal. Methods GeoMech. 45 (10), 1405–1436.
Lu, N., Likos, W.J., 2004. Unsaturated Soil Mechanics, first ed. Wiley, USA.
Martinelli, M., 2016. Soil-water Interaction with Material Point Method. Double-Point Formulation. Technical Report. Report on EU-FP7 research project MPM-Dredge PIAP-GA-2012-324522.
Midas Gts, N.X., 2020. Midas GTS NX-computer software, v. 1.1. URL: https://globalsupport.midasuser.com/helpdesk/KB/View/32636343-midasgtsnxmanualsandtutorials. (Accessed 28 July 2022).
Mieremet, M.M.J., 2015. Numerical Stability for Velocity-Based 2-phase Formulation for Geotechnical Dynamic Analysis, Report 15-03. Reports of the Delft Institute of Applied Mathematics, Delft University of Technology, Delft, The Netherlands.
Padfield, C.J., Schofield, A.N., 1983. The development of centrifugal models to study the influence of uplift pressures on the stability of a flood bank. Geotechnique 33 (1), 57–66.
Redaelli, M., Cividini, A., Gioda, G., 2011. Influence of boundary conditions in a finite-element analysis of river levees. Int. J. GeoMech. 11 (5), 399–405.
Rohe, A., Allersma, H.G.B., 2000. Modelonderzoek naar het optreden van oprdijf-condities achter dijken, Report nr Geo, 490 a, Faculteit Civiele Techniek en Geowetenschappen. Delft Technische Universiteit Delft (in Dutch).
Sadeghirad, A., Brannon, R.M., Burghardt, J., 2011. A convected particle domain interpolation technique to extend applicability of the material point method for problems involving massive deformations. Int. J. Numer. Methods Eng. 86 (12), 1435–1456.
Steffen, M., Kirby, R.M., Berzins, M., 2008. Analysis and reduction of quadrature errors in the material point method (MPM). Int. J. Numer. Methods Eng. 76 (6), 922–948.
Sulsky, D., Chen, Z., Schreyer, H.L., 1994. A particle method for history-dependent materials. Comput. Methods Appl. Mech. Eng. 118 (1–2), 179–196.
Van, M.A., Koelewijn, A.R., Barends, F.B., 2005. Uplift phenomenon: model, validation, and design. Int. J. GeoMech. 5 (2), 98–106.
Yerro, A., Alonso, E.E., Pinyol, N.M., 2015. The material point method for unsaturated soils. Geotechnique 65 (3), 201–217.
Yerro, A., 2015. MPM Modelling of Landslides in Brittle and Unsaturated Soils. PhD thesis. Univestitat Politecnica de Catalunya, Spain.
Yerro, A., Girardi, V., Martinelli, M., Ceccato, F., 2022. Modelling unsaturated soils with the material point method. A discussion of the state-of-the-art. Geomech. Energy Environ. https://doi.org/10.1016/j.gete.2022.100343.
Zhang, D.Z., Ma, X., Giguere, P.T., 2011. Material point method enhanced by modified gradient of shape function. J. Comput. Phys. 230 (16), 6379–6398.

Dr. Veronica Girardi is a Post Doc at the Department of Civil, Environmental and Architectural Engineering of the University of Padua, Italy. She obtained MSc degree in 2017 and PhD degree in 2022 from the same university. During the PhD, she developed an unsaturated MPM formulation to describe the behavior of water retaining geo-structure and applied the formulation to study failure and post failure behavior of river levees under transient hydraulic loads. She is actively involved in the activities of an international research community in charge of developing the MPM research software Anura3D (https://github.com/Anura3D/Anura3D_OpenSource). Since 2020, she is part of a national research team working on the project entitled "Risk assessment of earth dams and river embankments to earthquakes and floods", funded by Italian Ministry of Education, University and Research (MIUR). Her research interests cover numerical methods in geotechnical engineering, MPM, slopes safety assessment, tailing dams, monitoring techniques of natural slopes and water retaining geo-structure.

Please cite this article as: Girardi V et al., Failure of levees induced by toe uplift: Investigation of post-failure behavior using material point method, Journal of Rock Mechanics and Geotechnical Engineering, https://doi.org/10.1016/j.jrmge.2022.07.015